Proceedings of Machine Learning Research – Under Review:1–13, 2026 Full Paper – MIDL 2026 submission

BETA: Resting-state fMRI Biotypes For tDCS Efficacy in Anxiety Among Older Adults At Risk For Alzheimer's Disease

Skylar E. Stolte[1,2,3*] skylastolte4444@ufl.edu
Junfu Cheng[4*] junfu.cheng@ufl.edu
Chintan Acharya[1] chintan.acharya@ufl.edu
Lin Gu[5] rin.tani.e8@tohoku.ac.jp
Andrew O'Shea[3] aoshea@phhp.ufl.edu
Aprinda Indahlastari[2,3] aprinda.indahlas@phhp.ufl.edu
Adam J. Woods[3,6] adam.woods@utdallas.edu
Ruogu Fang[1,3,4†] ruogu.fang@bme.ufl.edu

[1] *J. Crayton Pruitt Family Department of Biomedical Engineering, University of Florida, United States*
[2] *Department of Clinical and Health Psychology, University of Florida, United States*
[3] *Center for Cognitive Aging and Memory, Department of Clinical and Health Psychology, McKnight Brain Institute, University of Florida, USA*
[4] *Department of Electrical and Computer Engineering, University of Florida, United States*
[5] *Research Institute of Electrical Communication, Tohoku University, Japan*
[6] *Behavioral and Brain Sciences, The University of Texas at Dallas, USA*

Editors: Under Review for MIDL 2026

Abstract

Anxiety is usually gauged by self-report, yet a single symptom level can reflect disparate neural circuitry. In Alzheimer's disease and related dementias (ADRD) this heterogeneity becomes a barrier to effective neuromodulation: some patients may benefit from transcranial direct-current stimulation (tDCS), while others may not. To overcome this obstacle, we introduced BETA (Biotypes for tDCS Efficacy in Anxiety), a data-driven pipeline that uses resting-state fMRI functional connectivity to derive anxiety subtypes that are intrinsically linked to tDCS response. A transformer-based variational autoencoder compresses high-dimensional connectivity into a 50-dimensional latent embedding that emphasizes networks implicated in cognitive aging and anxiety. A deep-embedded clustering loss, regularized by a clinically informed term that pulls together individuals who exhibit similar post-tDCS anxiety change, yields four distinct subtypes. Across all subtypes, disrupted coupling between sensory-processing and higher-order cognitive regions emerges as a common hallmark. Crucially, one cluster is resistant to frontal-lobe tDCS, whereas two clusters demonstrate significant anxiety reduction following stimulation. The responsive subtypes are defined by strengthened connectivity between the lateral occipital cortex—superior division (sLOC) and medial frontal cortex (MedFC), and between sLOC and the intracalcarine cortex (ICC). BETA demonstrates that fMRI-based subtyping can directly identify which patients are likely to benefit from tDCS, providing a concrete roadmap for precision psychiatry in ADRD and facilitating tailored therapeutic strategies for anxiety.

Keywords: Anxiety, tDCS, ADRD, functional MRI, biotypes

* Equal Contribution
† Corresponding Author

1. Introduction

Anxiety is one of the most frequently reported neuropsychiatric symptoms in individuals with Alzheimer's disease (AD) and related dementias (ADRD) (Ferretti et al., 2001; Porter et al., 2003; Patel and Masurkar, 2021). Beyond its symptomatic burden, anxiety has been implicated as both a risk factor for, and a catalyst of, disease progression in AD (Chemerinski et al., 1998; Becker et al., 2018). Consequently, early and precise anxiety interventions may attenuate neurodegeneration and improve quality of life in this vulnerable population.

Current clinical practice relies almost exclusively on self-reported questionnaires, clinical ratings, and historical information to diagnose and monitor anxiety (Penninx et al., 2021). These tools, while essential, are constrained by subjectivity: cultural nuances, individual insight, and context can all skew scores (Evans et al., 2013). Importantly, identical anxiety ratings can mask distinct underlying neurobiological circuits, undermining the fidelity of treatment decision-making (Rao et al., 2023). This phenomenological heterogeneity presents a substantial barrier to the deployment of targeted neuromodulation therapies such as trans-cranial direct-current stimulation (tDCS).

Resting-state functional magnetic resonance imaging (fMRI) offers a means to objectively probe the large-scale connectivity patterns that underpin anxiety. Prior work has successfully identified neuropsychiatric biotypes in younger adults with depression and anxiety (Drysdale et al., 2017; Tozzi et al., 2024), yet almost all such studies focus on younger cohorts, leaving a critical gap in our understanding of anxiety in older adults at risk for AD. The emergence of distinct anxiety biotypes could inform which patients are most likely to benefit from neuromodulation, thereby advancing precision psychiatry in AD.

To bridge this gap, we introduce **BETA** (**Biotypes for tDCS Efficacy in Anxiety**), a data-driven framework that integrates resting-state fMRI with a transformer-based variational autoencoder (t-VAE) and a clinical-outcome regularization term. BETA first learns a 50-dimensional latent representation of functional connectivity that captures the canonical networks implicated in cognitive aging and anxiety—namely, the Cingulo-Opercular Network (CON), Frontoparietal Control Network (FPCN), Default Mode Network (DMN), medial frontal cortex, cerebellum, motor cortex, and visual systems—using NeuroSynth-derived masks (Yarkoni et al., 2011). The resulting latent space is then subjected to deep-embedded clustering, iteratively refining cluster assignments while enforcing proximity between participants who exhibit similar anxiety change following frontal-lobe tDCS. This joint optimization yields four distinct anxiety biotypes.

Our work is the first to identify biotypes for tDCS efficacy for anxiety, and it advances precision neuromodulation in three concise steps:

- **Novel biotype discovery.** Four distinct anxiety biotypes are isolated from resting-state fMRI of older adults at risk for Alzheimer's disease, which is an under-studied population, with each biotype exhibiting a different pattern of response to frontal-lobe tDCS.
- **Intervention response prediction.** Two of the biotypes demonstrate marked anxiety relief after tDCS, one shows resistance, and the remaining groups occupy intermediate positions—providing a data-driven way to anticipate treatment outcomes from imaging alone.

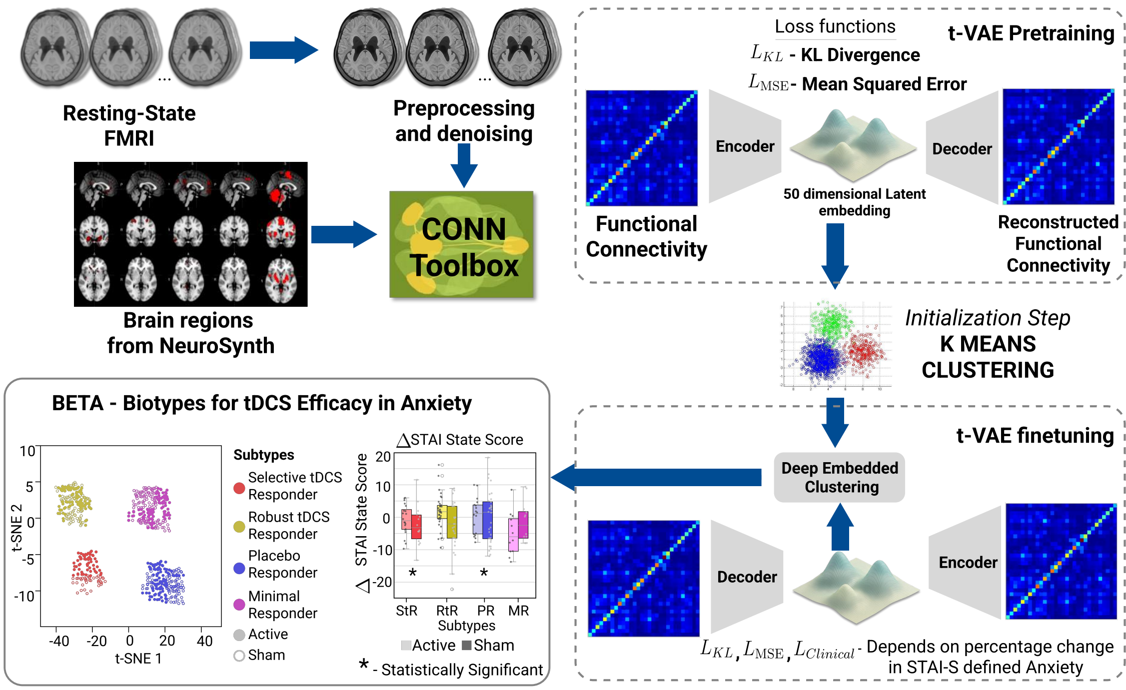

Figure 1: Overview of the BETA pipeline. The BETA pipeline embeds resting-state connectivity into a clinically informed latent space using a transformer-based VAE and deep embedded clustering, yielding distinct anxiety biotypes with differential sham and active tDCS responses.

- **Clinical decision support.** The biotype assignments are mapped to a simple, actionable tDCS recommendation schema, offering a proof–of–concept framework for individualized neuromodulation in geriatric anxiety.

2. Methodology

2.1. Dataset

This study used data from a randomized, double-blind trial: The Augmenting Cognitive Training in Older Adults study (ACT; clinicaltrials.gov NCT02851511). ACT examined the impact of transcranial direct-current stimulation (tDCS) combined with cognitive training (CT) on cognitive function in healthy older adults aged 65–89. Exclusion criteria comprised any neurological disorder, cognitive impairment, opportunistic brain infection, major psychiatric illness, unstable or chronic medical condition, MRI contraindication, impaired motor response, GABA-ergic medication use, or left-handedness. The protocol was IRB-approved and all participants provided written informed consent. Two research centers performed data acquisition on 3-T Siemens scanners (64-channel head coil at the primary site, 32-channel head coil at the secondary site). Both sites used earplugs to attenuate scanner noise and foam padding to limit head motion. After removing individuals with missing anxiety or fMRI data, the final sample included 199 participants (mean age = 71.27 ± 4.53 years; 61 males and 138 females). The sample comprised 99 Sham tDCS and 100 Active tDCS participants.

The State–Trait Anxiety Inventory (STAI) provides a self-report measure of anxiety with 20 items measuring "state" anxiety (STAI–S) and another 20 for "trait" anxiety (STAI–T) (Spielberger et al., 1999), each with a score range of 20 to 80. We collected participants' STAI state score at baseline and post-intervention (12 weeks after screening) time points.

2.1.1. tDCS Intervention

Participants received twelve weeks of tDCS-paired CT. Conventional tDCS was delivered at 2 mA intensity using two 5×7 cm^2 saline-soaked Soterix sponge electrodes over the F3-F4 locations (dorsolateral prefrontal cortex). The tDCS trial was double-blind: active and sham arms received identical setups, and allocation was concealed from both participants and experimenters. Each 40-min CT session began with 20 min of active tDCS. Active stimulation consisted of 2mA for 20 min with 30 s current ramp-up/down; sham stimulation was 2mA for 30 s with identical ramp-up/down, producing the same sensory experience while lacking a biologically meaningful effect.

2.1.2. Data Preprocessing and ROI Definition

Resting-state data were preprocessed in CONN (MATLAB 2022b) using standard steps including realignment, slice-timing correction, segmentation, co-registration, normalization to MNI space, and 8-mm smoothing; one participant was excluded for excessive motion. Regions of interest were defined using NeuroSynth activation maps (Yarkoni et al., 2011) associated with cognitive aging and anxiety (Waner et al., 2023; Takagi et al., 2018), thresholded and binarized to produce data-driven masks spanning Cingulo-Opercular, Frontoparietal Control, Default Mode, medial frontal, cerebellar, motor, and visual networks. These ROIs were used in CONN to extract pairwise functional connectivity (Pearson correlation, Fisher z-transformed).

2.2. Deep Embedded Clustering Pipeline

The pipeline compresses each subject's full resting-state functional connectivity (FC) matrix into a latent representation that preserves both anxiety-related network structure and tDCS response, using four tightly integrated stages.

2.2.1. Feature extraction with a transformer-based variational auto-encoder (t-VAE)

Variational autoencoders (VAEs) have long been used to summarize high-dimensional fMRI time-series and connectivity maps (Kim et al., 2021; Han et al., 2019; Qiang et al., 2021). In this work, we replace the conventional feed-forward encoder with a transformer architecture, allowing the model to learn long-range dependencies that are characteristic of distributed resting-state networks. The encoder comprises four transformer blocks (each with eight self-attention heads and a 64-dimensional hidden state). After the transformer stack a linear projection collapses the concatenated hidden states to a 50-dimensional latent vector z. The decoder mirrors this architecture and reconstructs the full functional-connectivity matrix from z. We selected a latent dimensionality of 50 based on a nested cross-validation sweep over 20, 50, 80 dimensions; the reconstruction error plateaued at 50, indicating sufficient capacity without over-fitting (Waswani et al., 2017). This latent space serves as the input to the subsequent embedded clustering stage.

2.2.2. Initial Clustering

After the transformer-based VAE has produced a 50-dimensional latent representation $\mathbf{z}$ for each subject, we initialize a set of five cluster centroids by running standard k-means on the latent vectors. This "warm-start" provides a meaningful segmentation of the data that accelerates convergence and stabilises the optimisation trajectory (Drysdale et al., 2017).

2.2.3. Joint Optimization

During training the centroids and the encoder–decoder parameters are updated *jointly* in a single back-propagation loop. The objective function minimises three terms:

i **Reconstruction loss** $\mathcal{L}_{\text{MSE}}$, the mean-squared error between the input FC matrix and the matrix reconstructed from $\mathbf{z}$.

ii **KL divergence** $\mathcal{L}_{\text{KL}}$, which regularises the distribution of $\mathbf{z}$ toward a standard normal prior (Kullback and Leibler, 1951).

iii **Clinical-informed regularisation** $\mathcal{L}_{\text{clinical}}$, a kernel-based penalty that encourages participants with similar changes in the State-Trait Anxiety Inventory (STAI-S) to occupy nearby locations in the latent space (Hofmann et al., 2008). Details of this specially designed loss in this paper is elaborated in Section 2.2.4.

The overall loss is therefore

$$\mathcal{L}_{\text{Total}} = \underbrace{\mathcal{L}_{\text{MSE}}}_{\text{reconstruction error}} + \underbrace{\mathcal{L}_{\text{KL}}}_{\text{KL divergence}} + \beta \underbrace{\mathcal{L}_{\text{Clinical}}}_{\text{clinical-informed loss}} \tag{1}$$

where β weights the influence of the clinical term; we set $\beta = 0.1$ after a brief grid search. By optimizing the centroids and the VAE parameters simultaneously, the model learns a latent space that is simultaneously faithful to the neuroimaging data and aligned with the observed clinical the response to tDCS.

2.2.4. Clinical-Informed Regularization

Because the intervention period is only twelve weeks, we focus on the STAI-S score and define the relative change

$$x_i = \frac{\text{STAI}_{i,\text{post}}}{\text{STAI}_{i,\text{pre}}}, \tag{2}$$

where $\text{STAI}_{i,\text{pre}}$ and $\text{STAI}_{i,\text{post}}$ are the baseline and post-tDCS scores for subject i. Participants whose baseline STAI–S exceeds 38 are considered to have moderate/severe state anxiety symptoms and clinically relevant anxiety (CRAL).

For every pair of participants (i, j) in the current mini-batch B, we compute a kernel similarity

$$w_{ij} = \exp\Big(-\frac{|x_i - x_j|^2}{2\sigma^2}\Big), \tag{3}$$

with σ fixed to 1.0. The clinical-informed loss is then the weighted sum of squared latent distances:

$$\mathcal{L}_{\text{clinical}} = \frac{1}{|B|} \sum_{(i,j)\in B} w_{ij} \, \|\mathbf{z}_i - \mathbf{z}_j\|_2^2, \tag{4}$$

where $\mathbf{z}_i$ denotes the 50-dimensional latent representation of subject i. This term penalizes large latent separations between participants who exhibit similar changes in STAI-S, encouraging the embedding to encode treatment efficacy (Hofmann et al., 2008).

The total training objective (Eq. (1)) therefore consists of the reconstruction loss, the KL divergence, and the weighted clinical regulariser, as shown in the previous section. The hyper-parameter $\beta = 0.1$ was chosen by a brief grid search to balance fidelity to the imaging data against adherence to the clinical signal. By optimizing $\mathcal{L}_{\text{clinical}}$ jointly with the VAE and clustering losses, the model learns a latent space that is simultaneously structured by the brain's functional connectivity and predictive of the individual response to frontal-lobe tDCS.

2.3. Model Training

Model optimization used Adam (Kingma and Ba, 2014) and followed a two-stage training procedure. In the variational autoencoder (VAE) stage, reconstruction was learned using a loss that combined Mean Squared Error (MSE) with KL divergence to regularize the latent space. The final clustering stage adopted a deep embedded clustering (DEC) objective (Xie et al., 2016), in which KL divergence measures the discrepancy between current cluster assignments and a sharpened target distribution. Throughout training, both active- and sham-tDCS participants were included to ensure that the model distinguished genuine treatment effects from minimal sham-related changes. Additional methodological detail is provided in the Supplementary Materials.

2.4. Inference

During inference, the BETA model operates on a single resting-state fMRI dataset. First, the pre-processed connectivity matrix is fed through the encoder of the pre-trained transformer based VAE, yielding a 50-dimensional latent vector $\mathbf{z}_{\text{new}}$. Next, the Euclidean distance between $\mathbf{z}_{\text{new}}$ and each of the five cluster centroids $\{\mathbf{c}_k\}_{k=1}^{5}$ is computed, and the biotype $k^* = \arg\min_k \|\mathbf{z}_{\text{new}} - \mathbf{c}_k\|_2$ is assigned. Because the STAI-S score is used only during training to weight the clinical-informed loss, it is unnecessary for inference; thus BETA can predict a subject's likelihood of responding to frontal-lobe trans-cranial direct-current stimulation solely from their fMRI-derived latent representation, enabling pre-trial stratification and personalized therapeutic recommendation.

2.5. tDCS Efficacy within Clusters

We quantified tDCS efficacy using the pre–post change in STAI-S scores, computed as ΔSTAI-S = STAI-S$_{\text{Pre}}$ − STAI-S$_{\text{Post}}$, such that positive values indicate reductions in state anxiety. We performed cluster-level pre–post evaluation for each cluster derived from the deep embedded clustering pipeline. We computed ΔSTAI-S for each participant and acessed normality within each subtype using the Shapiro–Wilk test. Depending on distributional properties, we performed either a one-sample t-test or a Wilcoxon signed-rank test, Then, for each of the biotypes we tested whether frontal-lobe tDCS produced a statistically significant change in anxiety relative to sham. Active–Sham differences were tested using parametric and nonparametric two-sample methods (Welch's t-test, Mann–Whitney U), or permutation testing for small samples in three levels of baseline state anxiety separately: (i) the entire cluster samples (n), (ii) participants with moderate or severe state anxiety (STAI-S > 38), and (iii) participants with minimal or mild state anxiety (STAI-S ≤ 38).

3. Experiments and Results

3.1. tDCS Efficacy within Clusters

We identified four clusters using our BETA pipeline after removing one small cluster with $n = 3$ due to very limited size, which will lead to lack of sufficient statistical power for meaningful inference. The remaining four clusters: Selective tDCS Responder, Robust tDCS Responder, Placebo Responder, and Minimal Responder subtypes—were retained for all subsequent analyses. The demographic and psychological profiles of these four clusters are presented in the supplementary material. Cluster level pre–post evaluation and Active–Sham difference evaluation results was summarized in as illustrated in Table 1.

The pre–post analyses showed that the Selective tDCS Responder and Placebo Responder subtypes demonstrated statistically reliable reductions in STAI-S among participants with moderate or severe baseline state anxiety, whereas the Minimal Responder and Robust tDCS Responder subtypes showed no significant STAI-S change. The Selective tDCS Responder subtype cluster shows the greatest clinical benefit, with participants who had moderate to severe baseline state anxiety exhibiting a large and statistically significant reduction in STAI-S scores under active tDCS (26.0 ± 6.08; $n = 3$). This reduction exceeds the minimal important difference of 10 points proposed by Corsaletti et al. (Corsaletti et al., 2014), indicating a clinically meaningful improvement.

In Active–Sham difference evaluation across the entire samples in four clusters, the Robust tDCS Responder subtype cluster showed statistically significant ($p = 0.02$) superior state anxiety symptoms reduction under Active stimulation with tDCS. In addition, the minimal/mild baseline anxiety subgroup of the Robust tDCS Responder subtype also shows a statistically significant ($p = 0.03$) Active–Sham advantage among participants confirming superior improvements under Active stimulation. In contrast, the Selective tDCS Responder and Minimal Responder subtypes did not show statistically significant evidence that active tDCS stimulation outperformed sham. The Placebo Responder subtype demonstrated numerically larger mean STAI-S reductions under sham tDCS stimulation, but these differences did not reach statistical significance. Detailed Active–Sham difference evaluation results are in the supplementary material.

Table 1: Pre–post change in State–Trait Anxiety Inventory–State (STAI-S) scores (ΔSTAI-S), stratified by baseline STAI-S severity, tDCS condition, and data-driven subtype. Values are reported as mean (SD), with sample sizes shown as n. Asterisks (*) denote statistically significant within-cluster pre–post changes ($p < .05$). Braces labeled with † indicate subtypes exhibiting a significant Active vs. Sham difference in STAI-S improvement ($p < .05$). Bolded values reflect reductions exceeding the minimal important difference of 10 points, indicating clinically meaningful improvement.

Subtype	**Selective tDCS Responder (n=39)**	**Robust tDCS Responder (n=68)**	**Placebo Responder (n=60)**	**Minimal Responder (n=29)**
Minimal/Mild Sham tDCS	-0.5 (6.50) $n = 14$	-2.7 (7.43) $n = 29$ †	0.9 (7.99) $n = 32$	-4.0 (8.47) $n = 12$
Minimal/Mild Active tDCS	0.1 (5.56) $n = 20$	1.8 (5.82) $n = 34$ †	-0.9 (5.73) $n = 18$	-1.2 (6.58) $n = 12$
Moderate/Severe Sham tDCS	**15.0** (2.83) $n = 2$	N/A $n = 0$	**12.8** (13.00) $n = 4$	2.5 (9.57) $n = 4$
Moderate/Severe Active tDCS	**26.0** (6.08)* $n = 3$	7.0 (11.47) $n = 5$	7.3 (6.95)* $n = 6$	3.0 (N/A) $n = 1$
All Sham tDCS	1.4 (8.07) $n = 16$	-2.7 (7.43) $n = 29$ †	2.2 (9.24) $n = 36$	-2.4 (8.91) $n = 16$
All Active tDCS	3.5 (10.47) $n = 23$	2.5 (6.81) $n = 39$ †	1.2 (6.93) $n = 24$	-0.8 (6.40) $n = 13$

3.2. Cluster-level differences in Functional Connectivity

Figure 2 presents the four functional connections that differ most significantly from the population mean for each biotype. Across the four connectivity-based subtypes, the most notable finding is that active tDCS produced a meaningful reduction in anxiety only in groups showing stronger networks linking the lateral occipital cortex, angular gyrus and frontal control regions—including the superior frontal gyrus, inferior frontal gyrus, middle frontal gyrus and precentral gyrus. These enhanced circuits characterized the Selective tDCS Responder and Robust tDCS Responder subtypes. Notably, the Robust tDCS Responder subtype was the only group to show a significant overall improvement with active tDCS compared to sham tDCS. The Selective tDCS Responder group showed some common features in the functional connectivity trends. While it did not reach statistical significance, there was a clinically meaningful (greater than 10-point) difference in active vs. sham tDCS in people with moderate/severe anxiety. Hence, the similarities in functional trends between these two groups may be indicative of brain functional connections that are more susceptible to improvement from tDCS intervention. Generally, hyperactive engagement within these networks was associated with tDCS responsiveness. These findings underscore that targeted tDCS interventions may be particularly effective for specific connectivity-based subtypes of anxiety.

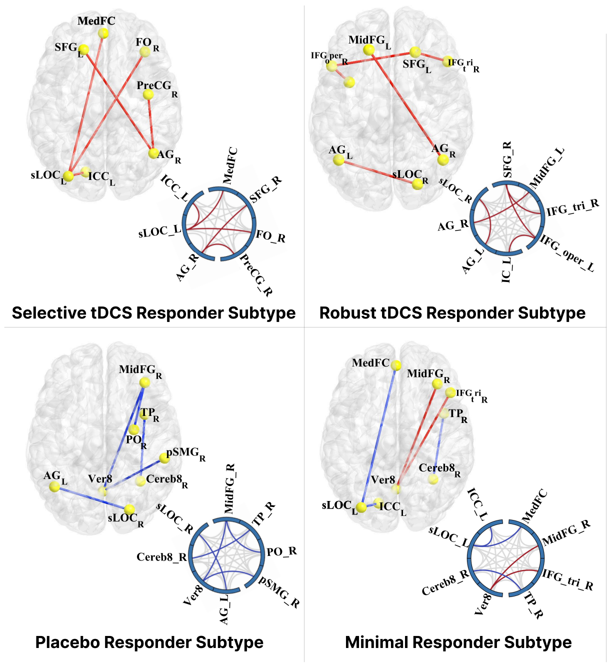

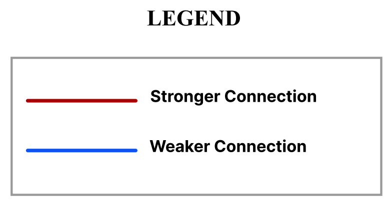

$sLOC_L$	Lateral Occipital Cortex, superior division Left	AG_L	Angular Gyrus Left
MedFC	Frontal Medial Cortex	$sLOC_R$	Lateral Occipital Cortex, superior division Right
ICC_L	Intracalcarine Cortex Left	TP_R	Temporal Pole Right
SFG_L	Superior Frontal Gyrus Left	$IFG_o per_R$	Inferior Frontal Gyrus, pars opercularis Left
AG_R	Angular Gyrus Right	$Cereb8_R$	Cerebellum 8 Right
FO_R	Frontal Operculum Cortex Right	$MidFG_R$	Middle Frontal Gyrus Right
$PreCG_R$	Precentral Gyrus Right	$pSMG_R$	Supramarginal Gyrus, posterior division Right
$IFG_t ri_R$	Inferior Frontal Gyrus, pars triangularis Right	PO_R	Parietal Operculum Cortex Right
Ver8	Vermis 8	IC_L	Insular Cortex Left
$MidFG_L$	Middle Frontal Gyrus Left	SFG_R	Superior Frontal Gyrus Right

Figure 2: Distinct hyper- and hypo-connectivity patterns across the four biotypes. Blue lines indicate weaker-than-average connections and red lines indicate stronger-than-average connections, revealing characteristic connectivity profiles for each subtype.

3.3. Ablation Analysis

We conducted an ablation analysis to assess the value of the clinical-informed loss term (L_{Clinical}). Models trained with and without this term were compared based on cluster-wise differences in anxiety change. The full model (with L_{Clinical}) yielded significant cluster differences (Welch's ANOVA: $p = 0.02$), whereas the ablation model showed no significant separation ($p = 0.10$). The full model also captured significant tDCS effects in the Robust tDCS Responder subtype cluster and clinically meaningful anxiety reductions in the Selective tDCS Responder subtype, whereas the ablation model produced no significant group differences in tDCS outcomes. These results show that the clinical-informed loss is crucial for shaping latent representations that capture differential tDCS responses. Without it, the t-VAE encodes general anxiety features, but adding L_{Clinical} guides the model toward representations better suited for analyzing targeted clinical interventions.

4. Discussions

This work derived fMRI-derived biomarkers of anxiety within older adults. Our findings indicate regions like the lateral occipital cortex (LOC) and the angular gyrus (AG) in anxiety. Previous research has supported that anxiety is often characterized by impaired functioning between regions for sensory processing (e.g., LOC,AG) and higher cognitive control (e.g. gyri in prefrontal regions) (Langhammer et al., 2024). The LOC is associated with visual processing (Li et al., 2020). Most anxiety work more commonly relates hyperactivity in the LOC with anxiety (Langhammer et al., 2024). The particular connection that occurred the most often between clusters was the LOC's connection to the Frontal Medial Cortex. The mechanism may possibly be via heightened fear processing and response (Li et al., 2020). However, our results indicate that there may be differential anxiety biotypes that correspond to reduced activity of the lateral occipital cortex. The reduced activity may possibly contribute to anxiety through a reduced ability to process environmental stimuli (van Dam and Chrysikou, 2021). The current study indicates that increased activity of the LOC is more associated with improvement in anxiety with tDCS. It seems like tDCS likely improves the ability of this region to exhibit inhibitory control. There may be a greater need to study how reduced activity in this region can be linked to anxiety so that interventions can be improved for these individuals. Another main area of interest is the AG, particularly its connection to the medial frontal gyrus. This connection has potential impacts on attention, memory, and language skills (De Boer et al., 2020). tDCS appears to be more likely to improve individuals who have hyperactivity in this region compared to hypoactivity. Previous research has focused on the AG as a target for tDCS to improve cognitive abilities related to dementia and memory (Hu et al., 2022). Our observations in the current study indicate that tDCS may improve cognitive performance related to the angular gyrus by helping regulate attention.

This study was limited by the dataset size. The original data source was based on relatively healthy older adults at risk of AD; it was not an anxiety dataset. Some clustering groups did not include enough data to compare individuals who had clinically significant anxiety across active and sham tDCS. For example,Robust tDCS Responder subtype cluster group did not include clinically relevant anxiety with sham tDCS. On average, each group was composed of about 10-20 percent clinically relevant anxiety.

5. Conclusions

This study demonstrates that resting-state fMRI connectivity can stratify individuals into biotypes with distinct responses to tDCS for anxiety. Our BETA pipeline processes new fMRI data to generate personalized intervention recommendations, allowing clinicians to target tDCS more effectively according to neuroimaging-derived subtypes and initial anxiety level. Participant in Robust tDCS Responder subtype are good candidates for protective tDCS against anxiety as a possible precursor to ADRD. Among all subtypes, the Selective tDCS Responder subtype stands out as the most clinically responsive group, whereas the Minimal Responder and Placebo Responder subtype cluster groups exhibited minimal or no improvement, indicating that biotype assignment can identify candidates for therapy and prioritize intervention strategies.

For future work, we aim to broaden the framework to include diverse participant profiles, additional clinical settings, and alternative neuromodulation modalities. The present work offers a foundational step toward precision psychiatry, underscoring the value of individualized, connectivity-based recommendations in optimizing anxiety interventions.

References

Eva Becker, Claudia Lorena Orellana Rios, Claas Lahmann, Gerta Ruecker, Joachim Bauer, and Martin Boeker. Anxiety as a risk factor of alzheimer's disease and vascular dementia. *The British Journal of Psychiatry*, 213(5):654–660, 2018.

Erán Chemerinski, Gustavo Petracca, Facundo Manes, Ramón Leiguarda, and Sergio E Starkstein. Prevalence and correlates of anxiety in alzheimer's disease. *Depression and anxiety*, 7(4):166–170, 1998.

Beatriz Fredegotto Corsaletti, Mahara-Daian Garcia Lemes Proença, Gianna Kelren Waldrich Bisca, Jéssica Cristina Leite, Laryssa Milenkovich Bellinetti, and Fábio Pitta. Minimal important difference for anxiety and depression surveys after intervention to increase daily physical activity in smokers. *Fisioterapia e Pesquisa*, 21(4):359–364, 2014.

DML De Boer, PJ Johnston, G Kerr, M Meinzer, and Axel Cleeremans. A causal role for the right angular gyrus in self-location mediated perspective taking. *Scientific reports*, 10(1):19229, 2020.

Andrew T Drysdale, Logan Grosenick, Jonathan Downar, Katharine Dunlop, Farrokh Mansouri, Yue Meng, Robert N Fetcho, Benjamin Zebley, Desmond J Oathes, Amit Etkin, et al. Resting-state connectivity biomarkers define neurophysiological subtypes of depression. *Nature medicine*, 23(1):28–38, 2017.

Spencer C Evans, Geoffrey M Reed, Michael C Roberts, Patricia Esparza, Ann D Watts, João Mendonça Correia, Pierre Ritchie, Mario Maj, and Shekhar Saxena. Psychologists' perspectives on the diagnostic classification of mental disorders: results from the who-iupsys global survey. *International Journal of Psychology*, 48(3):177–193, 2013.

Louise Ferretti, Susan M McCurry, Rebecca Logsdon, Laura Gibbons, and Linda Teri. Anxiety and alzheimer's disease. *Journal of geriatric psychiatry and neurology*, 14(1): 52–58, 2001.

Kuan Han, Haiguang Wen, Junxing Shi, Kun-Han Lu, Yizhen Zhang, Di Fu, and Zhongming Liu. Variational autoencoder: An unsupervised model for encoding and decoding fmri activity in visual cortex. *NeuroImage*, 198:125–136, 2019.

Thomas Hofmann, Bernhard Schölkopf, and Alexander J Smola. Kernel methods in machine learning. 2008.

Yueqing Hu, Yu Jia, Ying Sun, Yan Ding, Zhaoyang Huang, Chunyan Liu, and Yuping Wang. Efficacy and safety of simultaneous rtms–tdcs over bilateral angular gyrus on neuropsychiatric symptoms in patients with moderate alzheimer's disease: A prospective, randomized, sham-controlled pilot study. *Brain Stimulation*, 15(6):1530–1537, 2022. doi: 10.1016/j.brs.2022.11.009. URL https://pubmed.ncbi.nlm.nih.gov/36460293/.

Jung-Hoon Kim, Yizhen Zhang, Kuan Han, Zheyu Wen, Minkyu Choi, and Zhongming Liu. Representation learning of resting state fmri with variational autoencoder. *NeuroImage*, 241:118423, 2021.

Diederik P. Kingma and Jimmy Ba. Adam: A method for stochastic optimization. *Proceedings of the 3rd International Conference on Learning Representations (ICLR)*, 2014. URL https://arxiv.org/abs/1412.6980.

S. Kullback and R. A. Leibler. Information theory and statistics. *The Annals of Mathematical Statistics*, 22(1):79–86, 1951.

Till Langhammer, Kevin Hilbert, Dirk Adolph, Volker Arolt, Sophie Bischoff, Joscha Böhnlein, Jan C Cwik, Udo Dannlowski, Jürgen Deckert, Katharina Domschke, et al. Resting-state functional connectivity in anxiety disorders: a multicenter fmri study. *Molecular psychiatry*, pages 1–10, 2024.

Kun Li, Meng Zhang, Haisan Zhang, Xianrui Li, Feng Zou, Yufeng Wang, Xin Wu, and Hongxing Zhang. The spontaneous activity and functional network of the occipital cortex is correlated with state anxiety in healthy adults. *Neuroscience Letters*, 715:134596, 2020.

Palak Patel and Arjun Masurkar. Prevalence, risk factors, and impact of anxiety in the early stages of autopsy-confirmed alzheimer's disease: a retrospective study (1839). *Neurology*, 96(15_supplement):1839, 2021.

Brenda W. J. H. Penninx, Daniel S. Pine, Emily A. Holmes, and Andreas Reif. Anxiety disorders. *The Lancet*, 397(10277):914–927, 2021. doi: 10.1016/S0140-6736(21)00359-7. URL https://www.ncbi.nlm.nih.gov/pmc/articles/PMC9248771/.

Verna R Porter, William G Buxton, Lynn A Fairbanks, Tony Strickland, Susan M O'Connor, Susan Rosenberg-Thompson, and Jeffrey L Cummings. Frequency and characteristics of anxiety among patients with alzheimer's disease and related dementias. *The Journal of neuropsychiatry and clinical neurosciences*, 15(2):180–186, 2003.

Ning Qiang, Qinglin Dong, Hongtao Liang, Bao Ge, Shu Zhang, Yifei Sun, Cheng Zhang, Wei Zhang, Jie Gao, and Tianming Liu. Modeling and augmenting of fmri data using deep recurrent variational auto-encoder. *Journal of neural engineering*, 18(4):0460b6, 2021.

Vasudev R Rao, Pim Brouwers, Jeymohan Joseph, Collene Lawhorn, Lori AJ Scott Sheldon, and Dianne M Rausch. Biotypes of central nervous system complications in people living with human immunodeficiency virus (hiv): National institute of mental health perspectives on advancing the future of hiv healthcare. *The Journal of Infectious Diseases*, 227(Supplement_1):S58–S61, 2023.

Charles D Spielberger, Sumner J Sydeman, Ashley E Owen, and Brian J Marsh. *Measuring anxiety and anger with the State-Trait Anxiety Inventory (STAI) and the State-Trait Anger Expression Inventory (STAXI).* Lawrence Erlbaum Associates Publishers, 1999.

Yu Takagi, Yuki Sakai, Yoshinari Abe, Seiji Nishida, Ben J Harrison, Ignacio Martínez-Zalacaín, Carles Soriano-Mas, Jin Narumoto, and Saori C Tanaka. A common brain network among state, trait, and pathological anxiety from whole-brain functional connectivity. *Neuroimage*, 172:506–516, 2018.

Leonardo Tozzi, Xue Zhang, Adam Pines, Alisa M Olmsted, Emily S Zhai, Esther T Anene, Megan Chesnut, Bailey Holt-Gosselin, Sarah Chang, Patrick C Stetz, et al. Personalized brain circuit scores identify clinically distinct biotypes in depression and anxiety. *Nature Medicine*, pages 1–12, 2024.

Wessel O van Dam and Evangelia G Chrysikou. Effects of unilateral tdcs over left prefrontal cortex on emotion regulation in depression: evidence from concurrent functional magnetic resonance imaging. *Cognitive, Affective, & Behavioral Neuroscience*, 21(1):14–34, 2021.

Jori L Waner, Hanna K Hausman, Jessica N Kraft, Cheshire Hardcastle, Nicole D Evangelista, Andrew O'Shea, Alejandro Albizu, Emanuel M Boutzoukas, Emily J Van Etten, Pradyumna K Bharadwaj, et al. Connecting memory and functional brain networks in older adults: a resting-state fmri study. *GeroScience*, 45(5):3079–3093, 2023.

A Waswani, N Shazeer, N Parmar, J Uszkoreit, L Jones, A Gomez, L Kaiser, and I Polosukhin. Attention is all you need. In *NIPS*, 2017.

Junyuan Xie, Ross Girshick, and Ali Farhadi. Unsupervised deep embedding for clustering analysis, 2016. URL https://arxiv.org/abs/1511.06335.

Tal Yarkoni, Russell A. Poldrack, Thomas E. Nichols, David C. Van Essen, and Tor D. Wager. Large-scale automated synthesis of human functional neuroimaging data. *Nature Methods*, 8(8):665–670, 2011. doi: 10.1038/nmeth.1635. URL https://www.nature.com/articles/nmeth.1635.

Supplementary Material for BETA: Resting-state fMRI Biotypes For tDCS Efficacy in Anxiety Among Older Adults At Risk For Alzheimer's Disease

Skylar E. Stolte[1,2,3*] skylastolte4444@ufl.edu
Junfu Cheng[4*] junfu.cheng@ufl.edu
Chintan Acharya[1] chintan.acharya@ufl.edu
Lin Gu[5] rin.tani.e8@tohoku.ac.jp
Andrew O'Shea[3] aoshea@phhp.ufl.edu
Aprinda Indahlastari[2,3] aprinda.indahlas@phhp.ufl.edu
Adam J. Woods[3,6] adam.woods@utdallas.edu
Ruogu Fang[1,3,4†] ruogu.fang@bme.ufl.edu

[1] *J. Crayton Pruitt Family Department of Biomedical Engineering, University of Florida, United States*
[2] *Department of Clinical and Health Psychology, University of Florida, United States*
[3] *Center for Cognitive Aging and Memory, Department of Clinical and Health Psychology, McKnight Brain Institute, University of Florida, USA*
[4] *Department of Electrical and Computer Engineering, University of Florida, United States*
[5] *Research Institute of Electrical Communication, Tohoku University, Japan*
[6] *Behavioral and Brain Sciences, The University of Texas at Dallas, USA*

Editors: Under Review for MIDL 2026

1. Additional Dataset Details

The State-Trait Anxiety Inventory (STAI) has two subscales, each with a score range of 20 to 80. We collected participants' STAI state score at baseline and post-intervention (12 weeks after screening) time points, and change in State STAI scores for the Sham and Active tDCS groups and the corresponding individual trajectories are visualized in Figure 1. Change in STAI-S for the Sham and Active tDCS groups are summarized in Table 1.

* Equal Contribution
† Corresponding Author

Table 1: Sham and Active tDCS State STAI score change from pre-intervention to post-intervention. n: number of participants, *STAI-S*: STAI state score, *SD*: Standard deviation, *IQR*: Interquartile range

Measure	**Group**	**n**	**Mean**	**Median**	**SD**	**IQR**
Baseline STAI-S	Sham tDCS	99	27.33	25	7.58	9.50
Baseline STAI-S	Active tDCS	100	28.57	25	8.43	14.00
Baseline STAI-S	All	199	27.95	25	8.02	12.50
Post STAI-S	Sham tDCS	99	27.62	26	8.07	9.00
Post STAI-S	Active tDCS	100	26.68	24	7.58	11.25
Post STAI-S	All	199	27.15	25	7.82	9.00
STAI-S (Pre-Post)	Sham tDCS	99	-0.28	0	8.64	5.50
STAI-S (Pre-Post)	Active tDCS	100	1.89	0	7.77	7.00
STAI-S (Pre-Post)	All	199	0.81	0	8.27	6.00

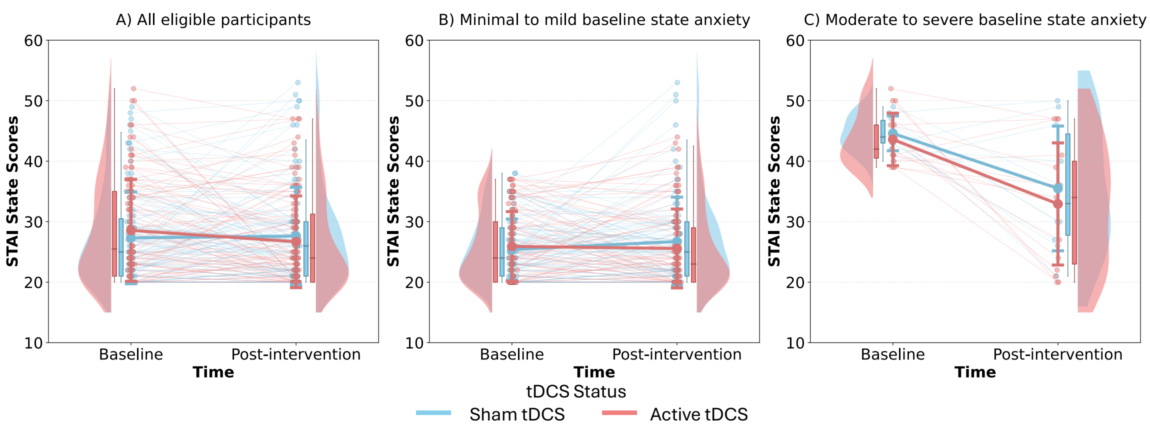

Figure 1: Spaghetti plots depicting individual State STAI score changes from baseline to post-intervention for Sham and Active tDCS participants, stratified by baseline anxiety severity.

2. Model Training Details

During optimization, we used the Adam optimizer with a learning rate of 1×10^{-5} for a maximum of 200 epochs. An initial warmup learning scheduler was used for 5 epochs to ensure a stable gradient during the beginning of the learning process. The model training loss balanced terms for KL Divergence and Mean Squared Error (MSE). The initial variational autoencoder stage learned how to reconstruct the functional correlation data. The final clustering model learned the optimal clustering using a clustering objective that was based off of deep embedded clustering approaches (Xie, Girshick, and Farhadi 2016). During both training schemes, the MSE loss refers to the ability to reconstruct the input data. The Variational Autoencoder applies KL divergence as the difference between the latent space and the normal distribution. The Deep Embedded Clustering using KL divergence as the difference between the current clustering assignments and a sharpened version of the clusters, as in (Xie, Girshick, and Farhadi 2016). Importantly, both active-tDCS and sham-tDCS participants were retained throughout training so that the model learned to distinguish genuine treatment effects from the negligible changes seen in the sham group.

3. Group-level Difference in Functional Connectivity

This experiment extracted the functional connectivity networks that were statistically different for each cluster compared to the population averages. The key outcome of this analysis is to learn how anxiety presents differently in each cluster. This information could provide potential insight into why the clusters may respond differently to tDCS interventions. We used one-sample t-testing to extract the functional connectivity differences that are significant for each cluster compared to the entire population. The pipeline used many one-sample t-tests for each cluster and functional connectivity network, so the false discovery rate (FDR) method (Benjamini and Hochberg 1995) was applied to correct for multiple comparisons.

Table 2 provides the corresponding quantitative details, including the mean connectivity value for each connection within every biotype and the 95% confidence interval for the population average. Together, these results demonstrate that each biotype exhibits a unique functional connectivity signature, highlighting the neurobiological heterogeneity across groups.

Table 2: Average functional connectivity strengths across four subtypes corresponding four clusters. ↑ and ↓ mean significantly stronger and significantly weaker connections for the given cluster, respectively. ROI Abbreviations and Full Region Names were listed in Table 3. The impact of tDCS across all participant in cluster: * = clinically significant anxiety improved with tDCS, ** = all anxiety improved with tDCS.

Subtype	**Selective tDCS Responder***	**Robust tDCS Responder****	**Placebo Responder**	**Minimal Responder**	**All Participants**
$sLOC_L - MedFC$	0.399 ↑	0.218	0.161 ↓	0.0930 ↓	0.219 ± 0.0380
$Ver8 - MidFG_R$	−0.0136 ↓	0.0220	−0.0381 ↓	0.197 ↑	0.0216 ± 0.0290
$IFG_{tri_R} - Ver8$	0.0332	0.0111	−0.0153 ↓	0.197 ↑	0.0301 ± 0.0310
$TP_R - Cereb8_R$	0.171 ↑	0.0885	0.0679	−0.0672 ↓	0.0783 ± 0.0310
$sLOC_L - ICC_L$	0.371 ↑	0.206	0.181 ↓	0.118 ↓	0.217 ± 0.0350
$SFG_L - AG_R$	0.461 ↑	0.450 ↑	0.317 ↓	0.404	0.398 ± 0.0340
$sLOC_L - FO_R$	0.264 ↑	0.155	0.127	0.0533 ↓	0.149 ± 0.0320
$AG_R - PreCG_R$	0.407 ↑	0.361 ↑	0.246 ↓	0.323	0.325 ± 0.0320
$MidFG_L - AG_R$	0.364 ↑	0.384 ↑	0.230 ↓	0.254 ↓	0.308 ± 0.0360
$IFG_{oper_L} - Cereb8_R$	0.214 ↑	0.0975	0.0628	−0.0225 ↓	0.0949 ± 0.0330
$AG_L - sLOC_R$	0.635 ↑	0.661 ↑	0.515 ↓	0.477 ↓	0.580 ± 0.0370
$IC_L - IFG_{oper_L}$	0.557 ↑	0.574 ↑	0.445 ↓	0.499	0.513 ± 0.0350
$SFG_R - IFG_{oper_L}$	0.655 ↑	0.668 ↑	0.517 ↓	0.530 ↓	0.592 ± 0.0400
$SFG_R - IFG_{tri_R}$	0.714	0.729 ↑	0.645	0.640 ↓	0.678 ± 0.0380
$Ver8 - pSMG_R$	0.0243	0.0319	0.00341 ↓	0.191 ↑	0.0453 ± 0.0280
$MidFG_R - PO_R$	-0.0702	−0.0340 ↑	−0.160 ↓	-0.103	-0.0842 ± 0.0320

Table 3: ROI Abbreviations and Full Region Names

Abbrev.	**Region Name**
$\mathrm{sLOC_L}$	Lateral Occipital Cortex, superior division Left
MedFC	Frontal Medial Cortex
$\mathrm{ICC_L}$	Intracalcarine Cortex Left
$\mathrm{SFG_L}$	Superior Frontal Gyrus Left
$\mathrm{AG_R}$	Angular Gyrus Right
$\mathrm{FO_R}$	Frontal Operculum Cortex Right
$\mathrm{PreCG_R}$	Precentral Gyrus Right
$\mathrm{IFG_{tri\ R}}$	Inferior Frontal Gyrus, pars triangularis Right
Ver8	Vermis 8
$\mathrm{MidFG_L}$	Middle Frontal Gyrus Left
$\mathrm{AG_L}$	Angular Gyrus Left
$\mathrm{sLOC_R}$	Lateral Occipital Cortex, superior division Right
$\mathrm{TP_R}$	Temporal Pole Right
$\mathrm{IFG_{oper\ R}}$	Inferior Frontal Gyrus, pars opercularis Right
$\mathrm{Cereb8_R}$	Cerebellum 8 Right
$\mathrm{MidFG_R}$	Middle Frontal Gyrus Right
$\mathrm{pSMG_R}$	Supramarginal Gyrus, posterior division Right
$\mathrm{PO_R}$	Parietal Operculum Cortex Right
$\mathrm{IC_L}$	Insular Cortex Left
$\mathrm{SFG_R}$	Superior Frontal Gyrus Right

4. Cluster-by-Cluster Results Across Baseline Severity Levels

In cluster level pre–post evaluation, for each cluster, change scores were tested against zero using one-sample t-tests when Shapiro–Wilk normality was not violated ($p < 0.05$) and Wilcoxon signed-rank tests otherwise. Subgroups in each cluster defined by baseline STAI S in clusters with $n = 1$ or $n = 0$ were not tested. For the Minimal/Mild baseline anxiety group, Active–Sham differences were evaluated using Welch's two-sample t-test (unequal variances) and the nonparametric Mann–Whitney U test, accompanied by assumption checks via Shapiro–Wilk normality tests and Levene's median-based variance test. Effect sizes were computed using Cohen's d, Hedges' g, and Glass's Δ. Because sample sizes were limited in the Moderate/Severe baseline group, condition differences were assessed using a two-sample permutation test on mean differences (10,000 permutations, two-sided), supplemented by the same normality and variance diagnostics and effect size estimates. The permutation test evaluates whether the observed Active–Sham difference could arise by chance by repeatedly shuffling group labels and recomputing the mean difference across thousands of random reallocations. Together, this approach ensured that each comparison was evaluated with statistical methods appropriate for the underlying sample size, distribution, and variance structure. The change of STAI-S across each cluster was illustrated in Figure 2.

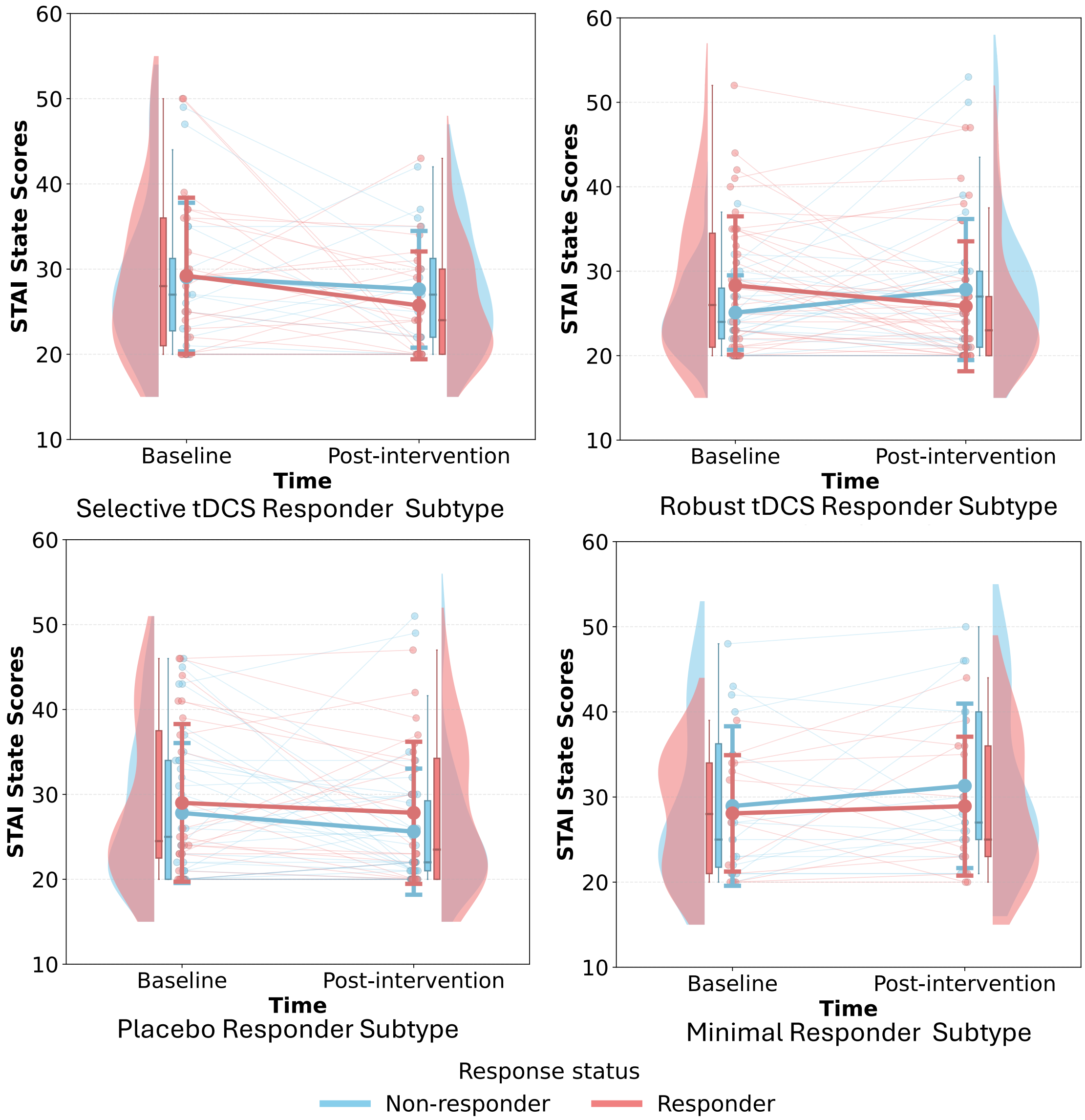

Figure 2: Pre–post changes in STAI-State scores across four clusters. Each panel shows baseline and post-intervention STAI-State scores for participants in the Selective tDCS Responder, Robust tDCS Responder, Placebo Responder, and Minimal Responder subtype clusters. Individual trajectories are displayed with light lines, overlaid with violin distributions and boxplots representing the score distributions at each time point. Colored trajectories indicate responder status (blue = non-responder; red = responder). Overall patterns highlight subtype-specific differences in anxiety reduction following the intervention.

Selective tDCS Responder Subtype. Individuals with moderate/severe baseline status show a very large improvement margin, with active tDCS producing gains more than ten points greater than sham. Selective tDCS Responder subtype cluster exhibits the strongest clinical improvement. This clinical response aligns with the Selective tDCS Responder subtype's densely interconnected fronto-parietal and medial-frontal network architecture, characterized by strengthened links among superior frontal, angular, occipital, and precentral regions—an organization that appears especially receptive to modulation by tDCS.

Robust tDCS Responder Subtype. Individuals show clear and statistically significant gains under active tDCS compared with sham, including reliable improvement in the minimal and mild baseline groups. Robust tDCS Responder subtype cluster demonstrates a moderate but consistent benefit across individuals receiving active stimulation (7.0 ± 11.47; $n = 5$). The observed pre–post reductions are consistent with the Robust tDCS Responder subtype's selectively strengthened fronto-parietal and frontal–temporal connections, a network configuration that may permit effective engagement by tDCS-driven neuromodulation.

Placebo Responder Subtype. Individuals demonstrate greater improvement during sham stimulation + cognitive training (CT) than active tDCS + CT, indicating sensitivity to CT rather than stimulation-dependent benefit. Placebo Responder subtype shows significant improvement under active tDCS (7.3 ± 6.95; $n = 6$) and notable reductions even in the sham group (12.8 ± 13.00; $n = 4$). Improvement in the absence of stimulation suggests strong expectancy or placebo effects.

Minimal Responder Subtype. Individuals exhibit little to no improvement under either sham or active tDCS, reflecting limited responsiveness across condition. Minimal Responder subtype cluster, in contrast, exhibits minimal clinical benefit. Among Selectiveanxiety participants, the reduction under active stimulation is small (3.0; $n = 1$), and in minimally anxious individuals, change scores remain modest or even negative across sham and active conditions.

4.1. Selective tDCS Responder Subtype

Minimal/Mild Baseline Group. Participants showed minimal pre–post improvement in both conditions, with no evidence of an Active benefit.

Table 4: Selective tDCS Responder Subtype (Minimal/Mild): Descriptive Statistics

Condition	n	Mean Change	SD
Sham	14	−0.50	6.50
Active	20	0.10	5.56

Moderate/Severe Baseline Group. Active participants showed a numerically larger reduction than Sham, but permutation testing indicated the effect was not statistically reliable.

Table 5: Selective tDCS Responder Subtype (Minimal/Mild): Statistical Tests

Test	Statistic	p-value
Welch's t-test	$t = 0.28$	0.781
Mann–Whitney U	$U = 148$	0.805
Cohen's d	0.07	—

Table 6: Selective tDCS Responder Subtype (Moderate/Severe): Descriptive and Permutation Results

Condition	n	Mean Change	SD	—
Sham	2	7.00	2.83	
Active	3	18.00	7.00	
Observed Difference (A–S)		+11.00		
Permutation p-value		0.1956		
Cohen's d		2.10 (unstable)		

All Participants. When pooling Minimal/Mild and Moderate/Severe baseline groups, Active stimulation produced a slightly larger mean reduction in STAI-State scores than Sham in the Selective tDCS Responder subtype, but this difference was not statistically reliable. Both Welch's two-sample t-test and the Mann–Whitney U test were nonsignificant, and the effect size was small.

Table 7: Selective tDCS Responder Subtype (All Participants): Active–Sham Statistical Tests

Test	Statistic	p-value
Welch's t-test	$t = 0.69$	0.4968
Mann–Whitney U	$U = 196$	0.7525
Cohen's d	0.21	—

4.2. Robust tDCS Responder Subtype

Minimal/Mild Baseline Group. This subtype showed the strongest and only statistically reliable Active–Sham difference among the Minimal/Mild participants. Active stimulation produced significantly greater symptom reduction than Sham across both parametric and nonparametric tests based on Mann-Whitney U test.

Moderate/Severe Baseline Group. Only Active participants were present ($n = 5$), so no condition comparisons could be conducted.

Table 8: Robust tDCS Responder Subtype (Minimal/Mild): Descriptive Statistics

Condition	n	Mean Change	SD
Sham	29	−2.38	7.93
Active	34	−6.68	9.57

Table 9: Robust tDCS Responder Subtype (Minimal/Mild): Statistical Tests

Test	Statistic	p-value
Welch's t-test	$t = 2.65$	**0.0105**
Mann–Whitney *U*	$U = 649$	**0.0309**
Cohen's d	0.59	—

All Participants. Across all participants in the Robust tDCS Responder subtype, Active stimulation produced a substantially larger mean reduction in STAI-State scores than Sham. This Active–Sham difference was statistically reliable in the Mann–Whitney U test, with a medium-to-large effect size.

Table 10: Robust tDCS Responder Subtype (All Participants): Active–Sham Statistical Tests

Test	Statistic	p-value
Welch's t-test	$t = 2.95$	**0.0046**
Mann–Whitney *U*	$U = 753$	**0.0197**
Cohen's d	0.73	—

4.3. Placebo Responder Subtype

Minimal/Mild Baseline Group. This subtype showed moderately larger improvement under Active stimulation, though results did not reach statistical significance.

Table 11: Placebo Responder Subtype (Minimal/Mild): Descriptive Statistics

Condition	n	Mean Change	SD
Sham	32	−3.25	6.75
Active	18	−7.11	8.98

Moderate/Severe Baseline Group. Active participants showed slightly smaller improvements than Sham, but permutation tests confirmed no reliable difference.

All Participants. When Minimal/Mild and Moderate/Severe participants were combined, Active and Sham conditions produced very similar mean pre–post changes in STAI-

Table 12: Placebo Responder Subtype (Minimal/Mild): Statistical Tests

Test	Statistic	p-value
Welch's t-test	$t = -0.90$	0.135
Mann–Whitney U	$U = 259$	0.129
Cohen's d	0.52	—

Table 13: Placebo Responder Subtype (Moderate/Severe): Descriptive and Permutation Results

Condition	n	Mean Change	SD
Sham	4	12.75	12.99
Active	6	7.33	11.47
Observed Difference (A–S)		−5.42	
Permutation p-value		0.3946	
Cohen's d		−0.56	

State in the Placebo Responder subtype. Neither Welch's two-sample t-test nor the Mann–Whitney U test showed a significant Active–Sham difference, and the overall effect size was small and slightly negative.

Table 14: Placebo Responder Subtype (All Participants): Active–Sham Statistical Tests

Test	Statistic	p-value
Welch's t-test	$t = -0.49$	0.6249
Mann–Whitney U	$U = 426.5$	0.9395
Cohen's d	−0.12	—

4.4. Minimal Responder Subtype

Minimal/Mild Baseline Group. Participants in the Minimal Responder Subtype exhibited modest reductions in STAI-State scores in both Sham and Active conditions, with no statistically significant difference between stimulation types. Both Welch's t-test and Mann–Whitney U test indicated nonsignificant effects.

Table 15: Minimal Responder Subtype (Minimal/Mild): Descriptive Statistics

Condition	n	Mean Change	SD
Sham	12	−4.00	8.47
Active	12	−1.17	6.58

Table 16: Minimal Responder Subtype (Minimal/Mild): Statistical Tests

Test	Statistic	p-value
Welch's t-test	$t = 0.92$	0.371
Mann–Whitney U	$U = 82$	0.581
Cohen's d	0.34	—

Moderate/Severe Baseline Group. Only Sham participants were present ($n = 3$, mean change = 5.33), so no Active–Sham comparison was possible.

All Participants. Across all participants in the Minimal Responder subtype, both Sham and Active conditions showed only modest pre–post changes, and Active stimulation did not outperform Sham. Welch's two-sample t-test and the Mann–Whitney U test were nonsignificant, with a small effect size.

Table 17: Minimal Responder Subtype (All Participants): Active–Sham Statistical Tests

Test	Statistic	p-value
Welch's t-test	$t = 0.54$	0.5960
Mann–Whitney U	$U = 117$	0.5822
Cohen's d	0.19	—

4.5. Demographic and Psychological Profiles of Four Clusters

We identified four clusters reflecting distinct demographic and psychological profiles (Table 18). Based on prior work showing strong depression–anxiety comorbidity (Kessler et al. 2008); (Lamers et al. 2011), we included BDI-II subscales to capture shared affective variance that may influence connectivity patterns. Two clear demographic and psychological profiles patterns emerged among the four clusters. The Minimal Responder and Selective tDCS Responder subtypes cluster groups had more female participants and showed higher baseline STAI and BDI-II scores. In contrast, the Robust tDCS Responder and Placebo Responder subtypes were the groups with largest participant numbers, with moderate symptoms and balanced sex ratios.

Table 18: Demographic, clinical, and connectivity characteristics across the four data-driven clusters. n = number of participants; SD = standard deviation. BDI-II subscales include: Somatic (physical/vegetative symptoms), Affective (emotional symptoms), and Cognitive (self-critical or distorted thinking patterns).

Measure	**Selective tDCS Responder Subtype**	**Robust tDCS Responder Subtype**	**Placebo Responder Subtype**	**Minimal Responder Subtype**
n	39	68	60	29
Proportion (%)	19.60	34.17	30.15	14.57
Age (Mean (SD))	70.49 (3.46)	70.24 (4.25)	72.30 (4.81)	72.62 (5.43)
STAI-State Pre (Mean (SD))	29.15 (8.87)	26.94 (6.98)	28.28 (8.62)	28.55 (8.20)
STAI-Trait (Mean (SD))	28.56 (8.41)	27.91 (6.28)	28.37 (7.57)	29.07 (7.21)
BDI Total (Mean (SD))	2.59 (3.23)	2.76 (3.76)	3.65 (4.08)	4.72 (4.17)
BDI Somatic (Mean (SD))	1.64 (1.90)	1.78 (2.15)	2.38 (2.54)	3.10 (2.64)
BDI Affective (Mean (SD))	0.38 (0.75)	0.44 (0.84)	0.55 (0.98)	0.79 (1.01)
BDI Cognitive (Mean (SD))	0.56 (1.21)	0.54 (1.51)	0.72 (1.40)	0.83 (1.26)
Male (n)	10	23	22	6
Female (n)	29	45	38	23
Male (%)	25.64	33.82	36.67	20.69
Female (%)	74.36	66.18	63.33	79.31
Mean Red-Box Connectivity	0.3241	0.2889	0.2065	0.2365

References

Benjamini, Yoav and Drai Hochberg (1995). "Controlling the false discovery rate: A practical and powerful approach to multiple testing". In: *Journal of the Royal Statistical Society: Series B (Methodological)* 57.1, pp. 289–300.

Kessler, Ronald C et al. (2008). "Co-morbid major depression and generalized anxiety disorders in the National Comorbidity Survey follow-up". In: *Psychological medicine* 38.3, pp. 365–374.

Lamers, Femke et al. (2011). "Comorbidity patterns of anxiety and depressive disorders in a large cohort study: the Netherlands Study of Depression and Anxiety (NESDA)". In: *Journal of clinical psychiatry* 72.3, p. 341.

Xie, Junyuan, Ross Girshick, and Ali Farhadi (2016). *Unsupervised Deep Embedding for Clustering Analysis*. arXiv: 1511.06335 [cs.LG]. URL: https://arxiv.org/abs/1511.06335.